Hysteresis and return-point memory in colloidal artificial spin ice systems

A. Libál,[1] C. Reichhardt,[2] and C. J. Olson Reichhardt[2]
[1]*Faculty of Mathematics and Computer Science, Babes-Bolyai University, RO-400591 Cluj-Napoca, Romania*
[2]*Theoretical Division, Los Alamos National Laboratory, Los Alamos, New Mexico 87545, USA*
(Received 17 August 2011; revised manuscript received 22 June 2012; published 27 August 2012)

Using computer simulations, we investigate hysteresis loops and return-point memory for artificial square and kagome spin ice systems by cycling an applied bias force and comparing microscopic effective spin configurations throughout the hysteresis cycle. Return-point memory loss is caused by motion of individual defects in kagome ice or of grain boundaries in square ice. In successive cycles, return-point memory is recovered rapidly in kagome ice. Memory is recovered more gradually in square ice due to the extended nature of the grain boundaries. Increasing the amount of quenched disorder increases the defect density but also enhances the return-point memory since the defects become trapped more easily.

DOI: 10.1103/PhysRevE.86.021406 PACS number(s): 82.70.Dd, 75.10.Hk, 75.10.Nr, 75.60.Jk

I. INTRODUCTION

Frustration effects arise in many condensed and soft matter systems, such as when geometric constraints prevent collections of interacting elements such as spins or charged particles from simultaneously minimizing all pairwise interaction energies. One of the best known frustrated systems are the spin ices [1,2], named for their similarity to the frustrated proton ordering in water ice [3]. Spin ices have been realized in both two and three dimensions and exhibit interesting excitations such as effective magnetic monopoles [1,4]. More recently, artificial spin ices were created with arrays of nanomagnets [5–14], colloidal particles [15,16], and vortices in nanostructured superconductors [17]. In artificial ices, direct visualization of the microscopic effective spin configurations is possible, and system parameters such as interaction strength, doping, or the amount of quenched disorder can be controlled. Under a varying external field, changes in the microscopic configurations can be imaged and used to construct hysteresis loops [7–9,14], as shown for kagome ice where the motion, creation, and annihilation of topological defects along the hysteresis cycle were demonstrated [7]. Memory effects are generally associated with hysteresis, and in return-point memory (RPM), the system returns to the same *microscopic* configuration after completing a hysteresis loop [18–22]. Recently developed techniques show that in real magnetic materials, RPM occurs in strongly disordered samples and is absent for weak disorder when the system becomes too soft to remember its previous state [19,20,22]. Certain classes of $T = 0$ disordered spin systems, such as the random field Ising model [18], exhibit perfect RPM, while other systems require many loops to organize into a state with RPM [20,21]. In more general disordered systems, an RPM-like effect was recently observed in the form of random reorganization into a reversible state for assemblies of interacting particles subjected to a cyclic shear [23]. Insights into magnetic RPM may offer a better understanding of such reversible-irreversible transitions that have been observed in a broad range of systems [24].

Artificial spin ices are an ideal system for studying RPM since they exhibit hysteresis and the microscopic states can be visualized directly. The type of topological defect that forms and its mobility varies in different ice systems, ranging from mobile monopoles [7,9] in kagome ice to less mobile grain boundaries [6,17] in square ice, and this could modify the RPM behavior. To quantify this, we perform numerical simulations of hysteresis in artificial square and kagome spin ices constructed from colloids in double-well traps with varied amounts of quenched disorder. Our model was previously shown to capture the behavior of square and kagome ices [15,17], and the number and type of topological defects present can be controlled by changing the amount of quenched disorder [17]. We use molecular dynamics simulations to capture the motion of extended objects such as grain boundaries. Our work implies that RPM phenomena can be studied in general artificial spin systems where a spin degree of freedom can be defined, as well as in artificial spin ice systems where geometrical frustration of the effective spins is present. This provides a new method for exploring microscopic memory effects in condensed matter systems.

II. SIMULATION

We simulate an artificial spin ice of N charged colloidal particles trapped in an array of elongated double-well pinning sites that have two states determined by which well is occupied by the colloid. The dynamics of colloid i is governed by the overdamped equation of motion $\eta(d\mathbf{R}_i/dt) = \mathbf{F}_i^{cc} + \mathbf{F}_i^s + \mathbf{F}_{\rm ext}$, where the damping constant $\eta = 1$. The colloid-colloid interaction force has a Yukawa or screened Coulomb form, $\mathbf{F}_i^{cc} = -F_0 q^2 \sum_{i\neq j}^{N} \nabla_i V(R_{ij})$, with $V(R_{ij}) = (1/R_{ij})\exp(-\kappa R_{ij})\hat{\mathbf{r}}_{ij}$. Here $R_{ij} = |\mathbf{R}_i - \mathbf{R}_j|$, $\hat{\mathbf{R}}_{ij} = (\mathbf{R}_i - \mathbf{R}_j)/R_{ij}$, $\mathbf{R}_{i(j)}$ is the position of particle $i(j)$, $F_0 = Z^{*2}/(4\pi\epsilon\epsilon_0)$, Z^* is the unit of charge, ϵ is the solvent dielectric constant, q is the dimensionless colloid charge, $1/\kappa = 4a_0$ is the screening length, and a_0 is the unit of distance that is typically of order a micron. We neglect hydrodynamic interactions between colloids since we work in the low volume fraction limit and the colloids remain confined in the pins. The pinning force $\mathbf{F}_s$ arises from N_p elongated traps of length $l = 1.333a_0$, width $d_p = 0.4a_0$, and depth $f_p = 100F_0$. The pin ends are parabolic confining potentials with radius $r_p = 0.2a_0$. A cylindrical force restricts motion in the direction perpendicular to the long axis of the pinning site, and a barrier in the center of the pinning site is produced by a repulsive parabolic force of height f_r that creates two energy minima on

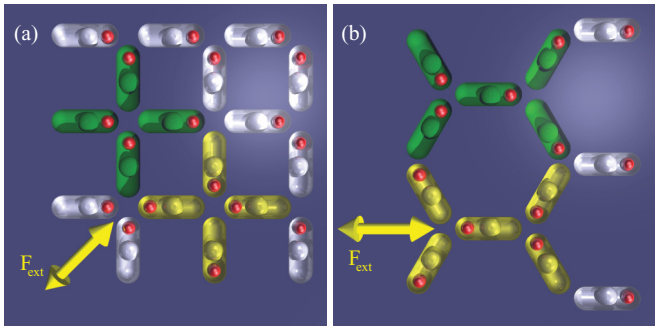

FIG. 1. (Color online) Schematic of a portion of the artificial ice samples. A charged colloid (dots) can sit in either end of each trap (lozenges). Dark green (light yellow) traps surround vertices that are in a positively (negatively) biased ground state. (a) Square ice, with $F_{\rm ext}$ applied at $\theta = 45^\circ$ from the x axis. (b) Kagome ice, with $F_{\rm ext}$ applied along the x axis.

either end of the pin [15]. For square ice the pins are arranged with $v = 4$ traps meeting at each vertex, while for kagome ice, $v = 3$ traps meet at each vertex [17], as shown in Fig. 1. The distance between adjacent vertices is $a = 2a_0$ and there are N_v vertices. Our square ice has 35×35 vertices ($N_v = 1225$) and $N_p = 2450$ elongated pins, while our kagome ice has 40×40 vertices ($N_v = 1600$) and $N_p = 2400$ elongated pins. Systems of larger size show the same behavior. Disorder is added to the system by increasing or decreasing f_r in individual pinning sites according to a normal distribution with mean $f_b = 1.0F_0$ and standard deviation σ. This is analogous to varied island coercive fields in the nanomagnetic system. We initialize the system by placing a colloid in one randomly selected end of each pinning site so that $N = N_p$. To construct a hysteresis loop we apply an external force $\mathbf{F}_{\rm ext} = F_{\rm ext}\hat{\mathbf{n}}$ uniformly to the sample, which for charged colloidal particles could be achieved using an external electric field. In the kagome ice $\hat{\mathbf{n}} = \hat{\mathbf{x}}$, while in the square ice $\hat{\mathbf{n}} = \sqrt{2}(\hat{\mathbf{x}} + \hat{\mathbf{y}})/2$, as illustrated in Fig. 1. For large enough $F_{\rm ext}$, the sample saturates into a biased ground state determined by the direction of $\mathbf{F}_{\rm ext}$. The two types of biased ground state vertices are illustrated for both ices in Fig. 1. We sweep $F_{\rm ext}$ from zero to a positive maximum value $F_{\rm max}$ at a rate of $\delta F_{\rm ext} = 0.005$ every 5000 simulation steps, then back down through zero to a negative maximum value $-F_{\rm max}$, and finally back up to zero to create one loop. Our results are unchanged for slower sweep rates using smaller values of $\delta F_{\rm ext}$. The initial curve is defined as the first sweep up of $F_{\rm ext}$ to $F_{\rm max}$ after the sample has been prepared in a random state.

III. RESULTS

We first show that our model captures the hysteretic behavior observed in artificial ice systems [7–9,19]. In the absence of quenched disorder or drive, we find ice-rule obeying states that are ordered ground states in the square ice [15] and disordered in the kagome ice. When we add quenched disorder with $\sigma > 0$, due to its lack of extensive degeneracy the square ice forms grain boundaries composed of non-ice-rule obeying vertices as shown in simulation [17] and experiment [6], while in kagome ice isolated non-ice-rule defects appear [7,17]. We define the reduced magnetization m as the projection

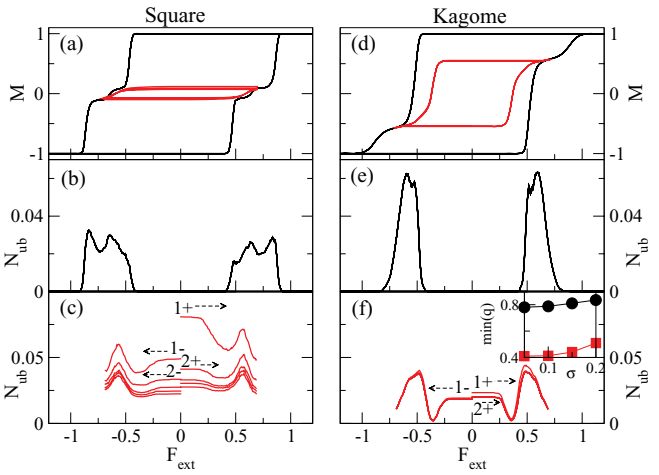

FIG. 2. (Color online) (a)–(c) Square ice sample with $\sigma = 0.1$. (d)–(f) Kagome ice sample with $\sigma = 0.1$. All curves are averaged over ten disorder realizations. (a) and (d) The reduced magnetization m vs $F_{\rm ext}$. Saturation occurs at $m = \pm 1.0$ when all the vertices are in biased states. Outer line: Saturated loop with $F_{\rm max} = 2.0$. Inner lines: Consecutive loops with $F_{\rm max} = 0.7$, below saturation. The initial curves are not shown. (b) and (e) Fraction of unbiased vertices $N_{\rm ub}$ vs $F_{\rm ext}$ for the saturated loop with $F_{\rm max} = 2.0$. (c) and (f) $N_{\rm ub}$ vs $F_{\rm ext}$ for repeated unsaturated loops with $F_{\rm max} = 0.7$, with cycle number n increasing from top to bottom. For clarity, we omit the horizontal lines connecting $F_{\rm ext} = \pm F_{\rm max}$ to $F_{\rm ext} = 0$. The first few half cycles are labeled; dotted arrows indicate sweep direction for the labeled curves. There is a much greater decrease in $N_{\rm ub}$ for the square ice than for the kagome ice. Inset of (f): $\min(q)$, the effective spin overlap in the $n = 2$ cycle, vs σ for (circles) kagome and (squares) square ice. Samples with stronger disorder have higher q values.

of the effective spin of each trap onto the driving direction, $m = N_v^{-1} \sum_{i=1}^{N_p} \mathbf{s}_i^{\rm eff} \cdot \hat{\mathbf{n}}$, where $\mathbf{s}_i^{\rm eff}$ is a unit vector defined to point from the empty end of the trap to the filled end of the trap. In Fig. 2(a) and 2(d) we plot the hysteresis loops for square and kagome ice samples with $\sigma = 0.1$. The outer curve is obtained with $F_{\rm max} = 2.0$, beyond the saturation level where $m = \pm 1$. We plot the fraction of unbiased vertices $N_{\rm ub}$ versus $F_{\rm ext}$ with $F_{\rm max} = 2.0$ in Fig. 2(b) and 2(e). The completely ordered biased states are destroyed only for $0.4 < |F_{\rm ext}| < 1.0$, close to the coercive fields at which the effective spin direction flips. The shape of the hysteresis loop and the peaks in the nonbiased defect density in Fig. 2(b) and 2(e) are in excellent agreement with the digitally constructed hysteresis loops produced in experiments on nanomagnetic kagome ice samples [7–9]. We find the same behavior for slower sweep rates using smaller values of $\delta F_{\rm ext}$ and also for larger samples, as shown in Fig. 3. The inner curves in Figs. 2(a) and 2(d) show consecutive hysteresis loops obtained below saturation with $F_{\rm max} = 0.7$, near the middle of the range of $F_{\rm ext}$ in which the largest number of defects appear. In Fig. 2(c) and 2(f) we plot $N_{\rm ub}$ versus $F_{\rm ext}$ for the unsaturated hysteresis loops. For the square ice, Fig. 2(c) shows that $N_{\rm ub}$ decreases with increasing n, where n is the number of loops performed, indicating that defect annihilation is occurring. For continued cycling beyond the number of loops shown in the figure, the system settles into a steady state. In the kagome ice, Fig. 2(f) shows that $N_{\rm ub}$ hardly changes from one cycle to the next, indicating that only

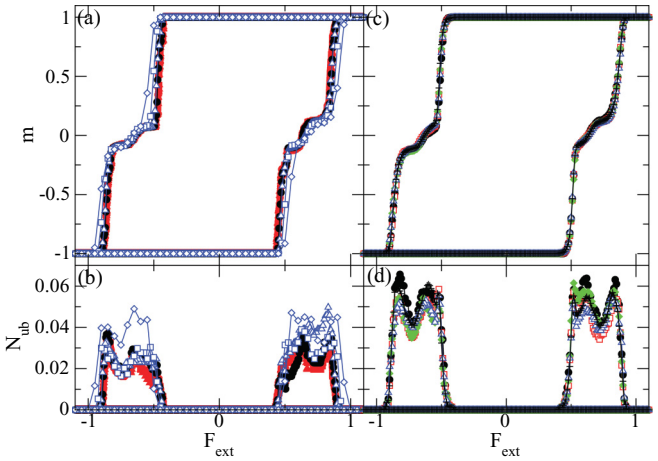

FIG. 3. (Color online) (a) Magnetization m vs F_{ext} and (b) number of defects N_{ub} vs F_{ext} for saturated loops with $F_{max} = 2.0$ obtained for the square ice system in Figs. 2(a)–2(c) using different sweep rates δF_{ext}. Black filled circles: $\delta F_{ext} = 0.005$, the rate used throughout the paper. Red filled symbols indicate slower sweep rates. Filled triangles: $\delta F_{ext} = 0.0005$; filled squares: $\delta F_{ext} = 0.0010$; filled diamonds: $\delta F_{ext} = 0.0025$. Blue open symbols indicate faster sweep rates. Open triangles: $\delta F_{ext} = 0.01$; open squares: $\delta F_{ext} = 0.025$; open diamonds: $\delta F_{ext} = 0.05$. The curves for $\delta F_{ext} = 0.005$ are nearly indistinguishable from curves obtained for slower sweep rates, indicating that we are working in the quasistatic regime in the paper. (c) Magnetization m vs F_{ext} and (d) number of defects N_{ub} vs F_{ext} for saturated loops with $F_{max} = 2.0$ obtained for the square ice system in Figs. 2(a)–2(c) with the same pinning density in samples of different size containing N_v pins. Black filled circles: $N_p = 3528$; red open squares: $N_p = 4802$; green filled diamonds: $N_p = 6272$; blue open triangles: $N_p = 7938$; black plus signs: $N_p = 9800$. The system size considered in Figs. 2(a)–2(c) is already large enough to be in the regime where no significant size dependence of the results appears.

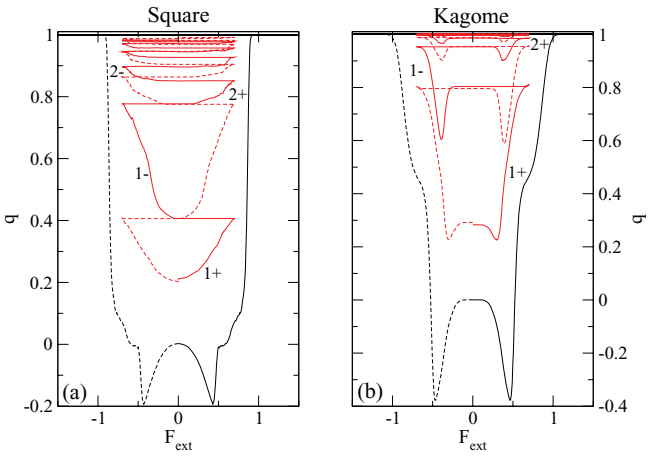

FIG. 4. (Color online) Effective spin overlap q vs F_{ext} during consecutive hysteresis loops averaged over ten disorder realizations for (a) a square ice sample with $\sigma = 0.1$ and (b) a kagome ice sample with $\sigma = 0.1$. Outer line: Saturated loop with $F_{max} = 2.0$, including the initial curve. Inner lines: Unsaturated loops with $F_{max} = 0.7$, with n increasing from bottom to top; the first few half loops are labeled. Solid lines: clockwise loops; dashed lines: counterclockwise loops. In the kagome ice, q approaches 1 after only a few cycles, while a much larger number of cycles are required before q approaches 1 in the square ice.

a small number of defects annihilate. For the saturated case with $F_{max} = 2.0$ shown in Fig. 2(b) and 2(e), the N_{ub} curves do not evolve under repeated looping since the sample loses all memory of the microscopic configuration near the coercive field once saturation is reached.

We quantify the RPM by measuring the overlap q in the effective spin configurations along a hysteresis loop [20,22] at equal values of F_{ext} after n complete cycles. For each trap, we define an effective spin $S_i = 1$ if the colloid is sitting in the right or top end of the trap, and $S_i = -1$ if the colloid is sitting in the left or bottom end of the trap. Writing the value of S_i after n cycles as $S_i^{(n)}$, we measure

$$q(F_{ext}) = N^{-1} \sum_{i=1}^{N} S_i^{(n-1)}(F_{ext}) S_i^{(n)}(F_{ext}). \qquad (1)$$

The term in the sum is 1 if the trap was biased in the same direction both before and after the complete cycle, and -1 if the colloid jumped to the other end of the trap. In Fig. 4(a) and 4(b) we plot q versus F_{ext} for both the saturated and unsaturated hysteresis curves in the square and kagome ices shown in Fig. 2(a) and 2(d). In the case of the saturated loops, q for the initial curve in Fig. 4(a) shows that since the sample was not initialized in a biased state, the initial configuration differs significantly from the effective spin configuration obtained one cycle later, but for $n = 2$ and above, $q = 1$, indicating perfect memory. For the unsaturated loops obtained with $F_{max} = 0.7$, q is low during the first cycle, but as n increases q gradually converges to a value just below $q = 1$. A comparison with Fig. 2(c) indicates that the increase in memory with increasing n is correlated with a decrease in N_{ub}, although for this value of F_{max} there are always some defected vertices present even after the system reaches a steady state in which the grain boundaries cease to evolve. The kagome ice in Fig. 4(b) shows a similar behavior except that q approaches 1 after only a few cycles, leading to a much faster establishment of RPM than in the square ice. In Fig. 2(f) we show that the number of defected vertices remains nearly constant in the kagome ice even under repeated cycling. This indicates that although the kagome ice defects do not annihilate, they are mobile during the first few cycles and then become pinned. Our results demonstrate that for the square ice, changes in the amount of RPM are primarily associated with the annihilation of defects, while in the kagome ice, RPM is suppressed by the motion of defects.

Although the number of defects N_{ub} in both types of ice increases with increasing disorder σ, the amount of RPM increases with increasing disorder. We illustrate this in the inset of Fig. 2(f) where we plot the value of q on the $n = 2$ plateau versus σ. A similar effect was observed for real magnetic systems and in spin simulations [19,20,22]. In our system, q increases with increasing disorder due to the stronger pinning of the domain walls in the square ice or of the individual defects in the kagome ice. In the square ice, the disorder prevents the domain walls from coarsening. It was previously shown that as the particle-particle interaction strength in our system is reduced, non-ice-rule obeying vertices begin to appear since their energetic cost decreases [15]. For noninteracting colloids, the sample is strongly disordered but

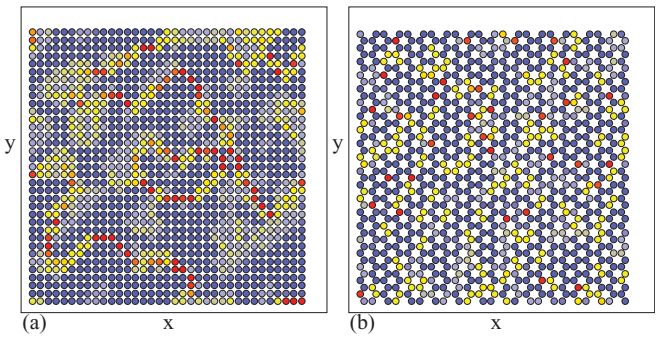

FIG. 5. (Color online) Vertices in (a) square ice and (b) kagome ice samples from Fig. 2 during repeated hysteresis cycles. Vertices are colored depending on how many cycles the vertex spends in a defect state, ranging from dark blue for never defected sites to dark red for permanently defected. (a) Motion and annihilation of defects occur near grain boundaries. (b) Individual defects move and are pinned independently without forming grain boundaries.

also has perfect RPM since the defected configurations are controlled only by the local disorder and are not modified by particle interactions. Thus we expect that in the experimental nanomagnetic artificial ices, when the coupling is reduced for increased spacing between the nanomagnets, the system should show increased or perfect RPM.

To illustrate the defect dynamics, in Fig. 5 we plot the vertices colored according to the number of hysteresis cycles each vertex spent as a defected site. Red vertices indicate locations where defects became trapped. Figure 5(a) shows that in the square ice, the defects organize into grain boundaries which move and coarsen under repeated hysteresis cycles. In Fig. 5(b) the kagome ice contains no grain boundaries but has a smaller fraction of intermediately colored vertices compared to the square ice since the isolated defects become trapped after only a few cycles. The square ice grain boundaries are less well pinned than the isolated kagome defects since they are extended objects. These mobile grain boundaries are responsible for the lower amount of RPM found in the square ice compared to the kagome ice. As the grain boundaries become trapped after repeated cycles, RPM increases and eventually saturates. The isolated kagome defects become trapped much more rapidly and their lower density contributes to the overall higher level of RPM in the kagome ice. The motion of individual defects in kagome ice has already been imaged in experiments; it would be interesting to observe whether these defects become localized within a few hysteresis cycles as we predict.

For most artificial ice systems, thermal effects are not relevant; however, thermal fluctuations can be significant in a colloidal system. We find that our results are robust against the addition of weak thermal disorder, and that for $T > 0$ there is only a slight reduction in the asymptotic value of q and a slight increase in the number of cycles required to reach a steady state. For higher temperatures, RPM is lost even when the system is cycled to saturation since the thermal fluctuations cause random effective spin flips that change the path on each cycle. There is also no increase in RPM under repeated cycles at higher temperature [22].

IV. SUMMARY

In summary, we have studied hysteresis and return-point memory effects for artificial square and kagome ices at the microscopic level. In the square ice for repeated unsaturated hysteresis loop cycles that extend to biases near the coercive field, the RPM increases with each cycle as the grain boundaries present in the sample coarsen and become pinned. In kagome ice the number of defects remains nearly constant under repeated hysteresis cycles and there is much higher RPM. Here individual defects hop rather than annihilating and are eventually pinned at sites with stronger disorder. The grain boundaries in the square ice are more mobile than the individual defects in the kagome ice since they are extended objects. Our results can be tested readily in different types of artificial ices and also could be studied in more general artificial spin systems.

ACKNOWLEDGMENTS

We thank the anonymous referees for their helpful comments. This work was carried out under the auspices of the National Nuclear Security Agency of the US Department of Energy at Los Alamos National Laboratory under Contract No. DE-AC52-06NA25396. A.L. was supported by a grant of the Romanian National Authority for Scientific Research, CNCS-UEFISCDI, project number PN-II-RU-TE-2011-3-0114.

[1] R. Moessner and A. P. Ramirez, Phys. Today **59**, 24 (2006).
[2] A. P. Ramirez, A. Hayashi, R. J. Cava, R. Siddharthan, and B. S. Shastry, Nature (London) **399**, 333 (1999); S. T. Bramwell and M. J. P. Gingras, Science **294**, 1495 (2001).
[3] L. Pauling, J. Am. Chem. Soc. **57**, 2680 (1935).
[4] C. Castelnovo, R. Moessner, and S. L. Sondhi, Nature (London) **451**, 42 (2008); L. D. C. Jaubert and P. C. W. Holdsworth, Nat. Phys. **5**, 258 (2009); D. J. P. Morris *et al.*, Science **326**, 411 (2009); S. T. Bramwell, S. R. Giblin, S. Calder, R. Aldus, D. Prabhakaran, and T. Fennell, Nature (London) **461**, 956 (2009).
[5] R. F. Wang *et al.*, Nature (London) **439**, 303 (2006); G. Möller and R. Moessner, Phys. Rev. Lett. **96**, 237202 (2006); X. Ke, J. Li, C. Nisoli, P. E. Lammert, W. McConville, R. F. Wang, V. H. Crespi, and P. Schiffer, *ibid.* **101**, 037205 (2008); C. Nisoli, J. Li, X. Ke, D. Garand, P. Schiffer, and V. H. Crespi, *ibid.* **105**, 047205 (2010); P. E. Lammert, X. Ke, J. Li, C. Nisoli, D. M. Garand, V. H. Crespi, and P. Schiffer, Nat. Phys. **6**, 786 (2010); J. Li, X. Ke, S. Zhang, D. Garand, C. Nisoli, P. Lammert, V. H. Crespi, and P. Schiffer, Phys. Rev. B **81**, 092406 (2010).
[6] J. P. Morgan, A. Stein, S. Langridge, and C. H. Marrows, Nat. Phys. **7**, 75 (2011).
[7] E. Mengotti, L. J. Heyderman, A. F. Rodríguez, F. Nolting, R. V. Hügli, and H.-B. Braun, Nat. Phys. **7**, 68 (2011).

[8] A. Schumann, B. Sothmann, P. Szary, and H. Zabel, Appl. Phys. Lett. **97**, 022509 (2010).

[9] O. Tchernyshyov, Nat. Phys. **6**, 323 (2010); S. Ladak, D. E. Read, G. K. Perkins, L. F. Cohen, and W. R. Branford, *ibid*. **6**, 359 (2010).

[10] Y. Qi, T. Brintlinger, and J. Cumings, Phys. Rev. B **77**, 094418 (2008); E. Mengotti, L. J. Heyderman, A. Fraile Rodríguez, A. Bisig, L. Le Guyader, F. Nolting, and H. B. Braun, *ibid*. **78**, 144402 (2008); N. Rougemaille *et al*., Phys. Rev. Lett. **106**, 057209 (2011).

[11] M. Tanaka, E. Saitoh, H. Miyajima, T. Yamaoka, and Y. Iye, Phys. Rev. B **73**, 052411 (2006).

[12] L. A. S. Mol, W. A. Moura-Melo, and A. R. Pereira, Phys. Rev. B **82**, 054434 (2010).

[13] Z. Budrikis, P. Politi, and R. L. Stamps, Phys. Rev. Lett. **105**, 017201 (2010); P. Mellado, O. Petrova, Y. Shen, and O. Tchernyshyov, *ibid*. **105**, 187206 (2010).

[14] K. K. Kohli, A. L. Balk, J. Li, S. Zhang, I. Gilbert, P. E. Lammert, V. H. Crespi, P. Schiffer, and N. Samarth, Phys. Rev. B **84**, 180412(R) (2011).

[15] A. Libál, C. Reichhardt, and C. J. Olson Reichhardt, Phys. Rev. Lett. **97**, 228302 (2006).

[16] Y. Han, Y. Shokef, A. M. Alsayed, P. Yunker, T. C. Lubensky, and A. G. Yodh, Nature (London) **456**, 898 (2008).

[17] A. Libál, C. J. Olson Reichhardt, and C. Reichhardt, Phys. Rev. Lett. **102**, 237004 (2009); M. L. Latimer, G. R. Berdiyorov, Z. L. Xiao, W. K. Kwok, and F. M. Peeters, Phys. Rev. B **85**, 012505 (2012).

[18] J. P. Sethna, K. Dahmen, S. Kartha, J. A. Krumhansl, B. W. Roberts, and J. D. Shore, Phys. Rev. Lett. **70**, 3347 (1993).

[19] M. S. Pierce *et al*., Phys. Rev. Lett. **94**, 017202 (2005).

[20] M. S. Pierce *et al*., Phys. Rev. B **75**, 144406 (2007).

[21] J. M. Deutsch and O. Narayan, Phys. Rev. Lett. **91**, 200601 (2003).

[22] H. G. Katzgraber and G. T. Zimanyi, Phys. Rev. B **74**, 020405(R) (2006).

[23] D. J. Pine, J. P. Gollub, J. F. Brady, and A. M. Leshansky, Nature (London) **438**, 997 (2005); L. Corte, P. M. Chaikin, J. P. Gollub, and D. J. Pine, Nat. Phys. **4**, 420 (2008); G. I. Menon and S. Ramaswamy, Phys. Rev. E **79**, 061108 (2009).

[24] N. Mangan, C. Reichhardt, and C. J. Olson Reichhardt, Phys. Rev. Lett. **100**, 187002 (2008); C. Reichhardt and C. J. Olson Reichhardt, *ibid*. **103**, 168301 (2009); S. Okuma, Y. Tsugawa, and A. Motohashi, Phys. Rev. B **83**, 012503 (2011).